# Metallomics

Integrated biometal science

www.rsc.org/metallomics

Volume 5 | Number 10 | October 2013 | Pages 1329–1460

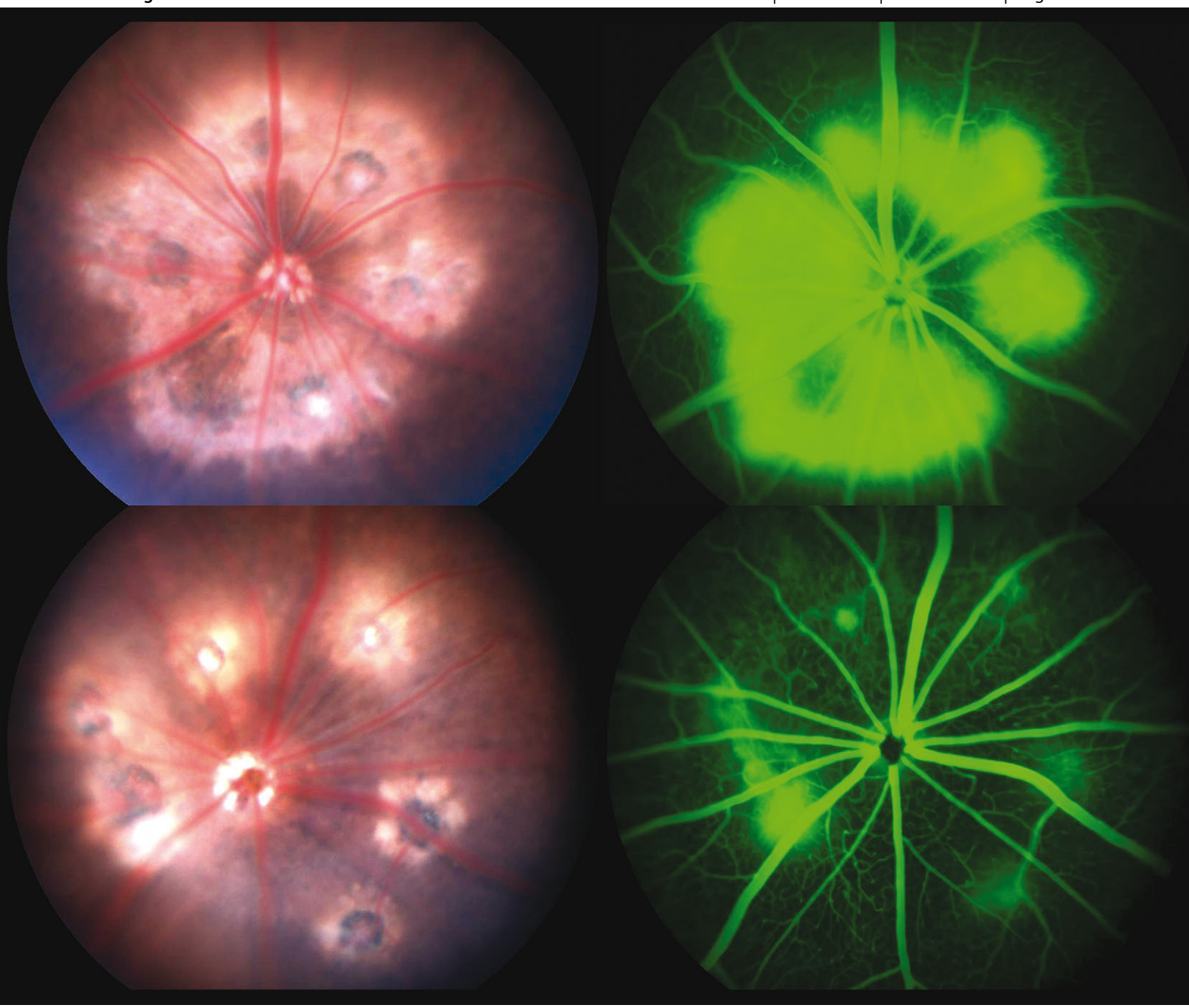

ISSN 1756-5901

**PAPER**

Jae-Young Koh *et al.*
Methallothionein-3 contributes to vascular endothelial growth factor induction in a mouse model of choroidal neovascularization

Indexed in MEDLINE!

RSC Publishing

1756-5901(2013)5:10;1-M

Metallomics

RSC Publishing

PAPER

View Article Online
View Journal | View Issue



Cite this: *Metallomics*, 2013, **5**, 1387

# Methallothionein-3 contributes to vascular endothelial growth factor induction in a mouse model of choroidal neovascularization†

Jeong A Choi,‡[a] Jong-uk Hwang,‡[b] Young Hee Yoon[b] and Jae-Young Koh*[ac]

In the present study, we investigated possible roles of the zinc (Zn)-binding protein metallothionein-3 (MT3) and cellular Zn in a mouse model of laser-induced choroidal neovascularization (CNV) using wild-type (WT) and MT3-knockout (KO) mice. Quantitative RT-PCR was used for the detection of MT3 mRNA. CNV was induced in mice between 8 and 12 weeks of age by disrupting the Bruch's membrane using an argon laser. Fundus photography and fluorescein angiography (FA) were performed 2 weeks following laser photocoagulation. The possible connection between MT3 and vascular endothelial growth factor (VEGF) expression was explored by quantifying VEGF levels in WT and MT3-KO mouse retinas by enzyme-linked immunosorbent assay. The role of Zn in VEGF expression was tested in WT and MT3-KO cells treated with pyrithione, with or without additional Zn, using immunoblotting and fluorescence photomicrography. Following laser-treatment, MT3-KO mice exhibited substantially smaller areas of CNV compared to WT mice. In addition, retinal angiograms revealed less severe fluorescein leakage in MT3-KO mice than in WT mice. On day 14 following the induction of CNV, VEGF expression was markedly increased in WT mice, but remained unchanged in MT3-KO mice. Consistent with the possible involvement of Zn released from MT3, raising intracellular Zn levels increased VEGF levels and activated its receptor, Flk-1, in both WT and MT3-KO retinal cells. Present results demonstrated that neural retinal cells express high levels of MT3, which might play a role in the process of CNV development. Moreover, Zn released from MT3 may contribute to VEGF induction.

Received 21st May 2013,
Accepted 30th July 2013

DOI: 10.1039/c3mt00150d

www.rsc.org/metallomics

## Introduction

Age-related macular degeneration (AMD) is the leading cause of blindness in developed countries among people over 55 years of age.[1] The overall prevalence of neovascular AMD and/or geographic atrophy in the US population 40 years and older is estimated to be 1.47% (95% confidence interval, 1.38–1.55%), with 1.75 million citizens having AMD.[2] Although the non-exudative (dry) form of AMD is more prevalent, catastrophic vision loss is more frequently associated with the exudative (wet) form, specifically due to complications of choroidal neovascularization (CNV).[3] Several risk factors have been implicated in the pathogenesis of CNV in exudative AMD, including complement activation, chronic intraocular inflammation, and Bruch's membrane dysfunction.[4–10] The induction of CNV is associated with the synthesis of numerous growth factors, including vascular endothelial growth factor (VEGF), platelet-derived growth factor (PDGF), and fibroblast growth factor (FGF).[11–15] Among these factors, VEGF has been shown to be a primary initiator of angiogenesis in the pathogenesis of CNV, and anti-VEGF antibodies have been used to treat CNV lesions in patients with wet AMD.[16,17] However, in spite of intensive treatment using anti-VEGF injections and close follow-up examination, a third of all wet AMD patients had poor vision of 20/200 or worse (legal blindness) at a mean 7.3 years after initiation of treatment.[18] This result suggests that new or adjunctive treatments of wet AMD are needed.

Despite several attempts to establish an animal model for human wet AMD, no model that exhibits all the features of human wet AMD exists. As an alternative, rupturing Bruch's membrane with laser photocoagulation has been widely utilized as a method for producing CNV in animals.[5,6,9] Although this model does not recapitulate all the features of human AMD, previous studies have found that it is useful for gaining insights

[a] *Neural Injury Research Center, Asan Institute for Life Sciences, University of Ulsan College of Medicine, Seoul, Korea*
[b] *Department of Ophthalmology, Asan Medical Center, University of Ulsan College of Medicine, Seoul, Korea*
[c] *Department of Neurology, Asan Medical Center, University of Ulsan College of Medicine, Seoul, Korea. E-mail: jkko@amc.seoul.kr; Fax: +82-2-483-5446; Tel: +82-2-3010-4127*

† This study was presented at the 42nd annual meeting of the Society for Neuroscience, October 2012, New Orleans, USA.

‡ Contributed equally to this research work and should be considered as first authors.

into the pathogenesis of new vessel growth from the choroid.[5,6,8] Hence, albeit incomplete, the rat/mouse laser model of CNV is currently considered the standard animal model of CNV.

Metallothioneins (MTs) are a group of low-molecular-weight (6–7 kDa), intracellular, cysteine-rich, metal-binding proteins that are expressed in many tissues.[19] Whereas metallothionein-1 (MT1) and metallothionein-2 (MT2) are ubiquitously expressed, metallothionein-3 (MT3), also known as growth inhibitory factor (GIF), is known to be expressed mainly in the central nervous system.[20] MT3 contains seven extra amino acids that allow it to accommodate more zinc (Zn) atoms than other MT isoforms.[21] Originally identified in the brain, MT3 is thought to exert primarily anti-oxidant, metal detoxification, and Zn homeostasis effects.[20] Although subsequent studies have revealed MT3 expression in various organs other than the brain,[22] its existence and role in the eye have not been reported. Since retina originates from neural tissue and hence is considered as a part of the CNS, it is likely that retina also expresses MT3.

The possible role of MT3 in angiogenesis or neovascularization has not yet been studied. However, it was demonstrated that changes in zinc levels may affect VEGF expression.[23] Considering that MT3 is likely the key source of intracellular zinc release in the brain and possibly in retina, we raised a hypothesis that MT3 may play a role in VEGF induction in pathological conditions such as CNV. Hence in the present study, we evaluated MT3 mRNA expression in the mouse eye and sought to elucidate possible roles of MT3 and Zn in the pathogenesis of CNV using wild-type (WT) and MT3-knockout (KO) mice in the laser-induced CNV model.

## Methods

### Chemicals

Pyrithione, *N*,*N*,*N*′,*N*′-tetrakis(–)(2-pyridylmethyl)-ethylenediamine (TPEN) and zinc chloride were obtained from Sigma (St. Louis, MO, USA).

### Animals

The animal experimental protocol was approved by the Internal Review Board for Animal Experiments of Asan Life Science Institute, University of Ulsan College of Medicine (Seoul, Republic of Korea). Mice of either gender between 8 and 12 weeks of age were used. MT3-KO ($MT3^{-/-}$) mice were produced as previously described.[24] Background mice were produced by mating male C57BL/6 and female SV129. WT and MT3-KO mice, generated by mating male and female heterozygous C57BL6/129Sv hybrid mice ($MT3^{+/-}$), were maintained in the Animal Facility of the University of Ulsan College of Medicine (Seoul, Republic of Korea). MT3 genotypes were determined by polymerase chain reaction (PCR) using the sense primer 5′-CTC TCT ACA GAG GCC CGG CAG TCA C-3′ (for WT) or 5′-GAC TGT GCC TTC TAG TTG CCA GCC ATC TG-3′ (for KO) and the antisense primer 5′-CAC AGT CCT TGG CAC ACT TCT CAC ATC CG-3′ (for both types). Animals were maintained at 24 °C ± 0.5 °C under a 12 h light–dark cycle and allowed free access to food and water before and after experiments. For all procedures, anesthesia was achieved by isoflurane inhalation (1.5% isoflurane in a 1 : 3 mixture of $O_2$ and $N_2O$), with the nose of the mouse placed into a small nose cone. Isoflurane induction was regularly performed by the same individual.

### Identification of MT3 in the eye

The presence of MT3 mRNA in the mouse eye was determined by quantitative real-time polymerase chain reaction (qPCR) in WT and MT3-KO mice. Total RNA was extracted from the mouse eye with TRIZOL Reagent (Invitrogen, Carlsbad, CA, USA). A QuantiTect Reverse Transcription Kit (Qiagen, Hilden, Germany) was used to generate cDNA according to the manufacturer's instructions. Samples were run in quadruplicate on a 7300 Real-Time PCR System (Applied Biosystems, Carlsbad, CA) using SYBR Premix Ex Taq Master Mix (Takara Bio, Japan) and forward and reverse primers for MT3. Thermocycling conditions included an initial denaturation at 95 °C for 5 s, followed by 40 cycles at 55 °C for 10 s and 72 °C for 31 s. Cycle threshold (Ct) values of the target MT3 were normalized to the Ct values of β-actin. Relative mRNA levels were quantified using the $2^{-\Delta\Delta Ct}$ method ($n = 3$).

### Induction of CNV

Laser photocoagulation (532 nm, 0.07 s, 50 μm; Novus Varia, Lumenis Inc., Yokneam, Israel) was performed on the right eye of each animal ($n = 21$ in the WT group; $n = 22$ in the KO group) by an operator blinded to the animal's genetic identity. A power setting of 200 mW was used for all eyes. Six laser spots were applied in a peripapillary distribution in a standardized fashion, approximately two to three disc diameters apart from the optic nerve head, using a slit-lamp delivery system and a coverslip as a contact lens. The appearance of a cavitation bubble, thought to correlate with the disruption of Bruch's membrane, was recorded. Spots with hemorrhagic complications were excluded from further evaluation. For measurement of the basal level of VEGF and morphologic analysis, four mice in each group that were not subjected to the laser photocoagulation procedure on either eye served as controls.

### Fluorescein angiography

Fourteen days after laser photocoagulation, fluorescein angiography (FA) was performed by an operator blinded to the genetic identity of the animal using a Micron III retinal imaging system (Phoenix Research Laboratories, Inc., Pleasanton, CA, USA). Photographs were captured through the objective lens optimized for a mouse eye, after intraperitoneal injection of 0.15 ml of 2% fluorescein sodium (Alcon Laboratories, Inc., Fort Worth, TX, USA). Two retina specialists, not involved in laser photocoagulation or angiography and blinded to the genetic identity of mice, evaluated the 2-week post-laser fluorescein angiograms in a single sitting. Lesions were graded using a previously established scheme as follows:[25] 0 (not leaky), faint hyperfluorescence or mottled fluorescence without leakage; 1 (questionable leakage), hyperfluorescent lesion without progressive increase in size or intensity; 2A (leaky), hyperfluorescence increasing in intensity but not in size; 2B (pathologically significant leakage),

 

hyperfluorescence increasing in intensity and size (WT $n$ = 5, spot = 52 and MT3-KO $n$ = 6, spot = 66).

### TFL-Zn staining for labile zinc

Twenty four hours after laser treatment, unfixed eye sections were stained with the zinc-specific fluorescent dye *N*-(6-methoxy-8-quinolyl)-*p*-carboxybenzoylsulphonamide (TFL-Zn, 0.1 mM in PBS, pH 8.0) (Calbiochem, La jolla, CA, USA) as previously described.[26]

### Histopathological examination of CNV

One day after angiography (day 15), eyes were enucleated and processed for histopathology. Complete washout of previously injected fluorescein was confirmed. Eyes were fixed in 4% paraformaldehyde and processed by cryostat sectioning using routine procedures. Eyes of WT and MT3-KO mice were sectioned at 10 μm intervals, stained with hematoxylin and eosin (H&E), mounted on glass slides, and examined for morphological differences.

### Measurement of CNV size and vascularity

The size and vascularity of CNV lesions were measured in captured FA images using the Micron III retinal imaging system. On day 14, FA images were captured during early (1–2 min), peak (3–4 min), and late (7–8 min) phases. Images were converted into common JPEG image format using manufacturer-provided software (StreamPix). Early-phase images that showed a definite demarcation line of CNV lesions were used to analyze the size of induced CNV lesions. Peak-phase FA images were utilized for analyzing the vascularity of CNV lesions. Abundant new vessels in the CNV lesions induce prominent fluorescein leakage in the angiogram, and therefore, the intensity of fluorescence (intensity of leakage) can be interpreted to correlate with the (neo)vascularity of CNV lesions. The relative strength of fluorescence in the CNV area was calculated by subtracting the intensity of fluorescence in adjacent major retinal vasculature. All analyses related to the size and vascularity of CNV were conducted using ImageJ version 1.44 software (Bethesda, MD, USA).

### ELISA for VEGF

On day 15 following laser injury, all eyes were enucleated after confirming complete washout of fluorescein sodium. Whole eyes were homogenized in phosphate-buffered saline (PBS) and sonicated. Following centrifugation, supernatants containing most soluble proteins were collected. VEGF protein levels in the supernatant were determined using an ELISA kit (Quantikine; R&D Systems, Minneapolis, MN, USA) that recognizes all splice variants (threshold of detection, 3 pg $ml^{-1}$). Absorbance values were obtained at 450 to 570 nm using an Emax spectrophotometer (Molecular Devices, Sunnyvale, CA, USA) and were normalized to total protein (Bio-Rad, Hercules, CA, USA). Measurements were performed in duplicate (WT CTL = 13, CNV = 7; KO CTL = 12, CNV = 5).

### Western blot analysis

Samples for immunoblotting were prepared by homogenizing whole eyes in RIPA buffer (20 mM Tris-Cl [pH 7.4], 150 mM NaCl, 1 mM EDTA, 1 mM EGTA, 1% Triton X-100, 2.5 mM sodium pyrophosphate, 1 μM $Na_3VO_4$, 1 μg $ml^{-1}$ leupeptin, and 1 mM phenylmethylsulfonyl fluoride). The lysates were centrifuged, and supernatants containing most soluble proteins were collected. Samples with equal amounts of protein were separated by sodium dodecyl sulfate-polyacrylamide gel electrophoresis (SDS-PAGE) and electroblotted onto polyvinylidene difluoride (PVDF) membranes (Millipore, Bedford, MA, USA) according to standard protocols. Membranes were blocked with 3% non-fat dried milk for 1 h and then incubated overnight at 4 °C with primary antibodies. The following primary antibodies were used: anti-VEGF, anti-Flk-1 (VEGF-R2), anti-phosphorylated Flk-1 (pFlk-1), and anti-HIF-1α (Santa Cruz Biotechnology, Santa Cruz, CA, USA). After washing, membranes treated with anti-VEGF and anti-HIF-1α were incubated with horseradish peroxidase (HRP)-conjugated goat anti-mouse IgG antibodies and then washed again. Membranes treated with anti-Flk-1 and anti-pFlk-1 were incubated with HRP-conjugated goat anti-rabbit IgG antibodies. All secondary antibodies were purchased from Thermo Fisher Scientific Incorporation. Immunoreactive proteins were visualized using Immobilon Western Chemiluminescent HRP Substrate (Millipore, Billerica, MA, USA), and their intensities were quantitatively analyzed by densitometry (ImageJ software).

### Relationship between intracellular Zn and VEGF in primary retinal cells and MT3 KO astrocytes

**Primary retinal cell culture.** Primary cell cultures, including neurons, astrocytes and photoreceptor cells, were generated from the retinas of newborn (postnatal day 3) Sprague–Dawley rats, as previously described.[27] Briefly, dissociated retinal cells were plated on poly-L-lysine and laminin-coated plates. The plating medium was based on Eagle's minimum essential medium (MEM; Gibco, CA, USA) supplemented with fetal bovine serum (FBS) and horse serum (10% [v/v] of each component) and penicillin–streptomycin (100 IU $ml^{-1}$–100 μg $ml^{-1}$; Lonza, Allendale, NJ, USA). Cytosine arabinoside (Ara C; 10 μM) was added 7 days after plating to halt the growth of non-neuronal cells. Retinal cultures were maintained at 37 °C in a humidified 5% $CO_2$ incubator and were used in experiments after culturing *in vitro* for 8 to 11 days.

**MT3-KO astrocyte culture.** Astrocytes were prepared from neonatal (2- to 3-day-old) MT3-KO mice. Cerebral cortices were removed, triturated by pipetting, and seeded into multiwell culture plates (BD Biosciences, NJ, USA) in Dulbecco's modified Eagle's medium (DMEM) supplemented with FBS and horse serum (7% [v/v] of each component) and penicillin–streptomycin (100 IU $ml^{-1}$ and 100 μg $ml^{-1}$, respectively). Primary cortical cultures were incubated at 37 °C in a humidified 5% (v/v) $CO_2$ atmosphere until cells reached confluence. The medium was changed every 3 days with rigorous shaking to remove contaminating nonadherent cells from adherent astrocytes. The resulting astrocyte-enriched cultures were ~95% pure, based on tests for glial fibrillary acidic protein (GFAP) immunoreactivity. All culture reagents except FBS (Hyclone, Logan, UT, USA) were purchased from Invitrogen (Carlsbad, CA, USA).

**Assessment of intracellular Zn levels.** Intracellular Zn levels were assessed by treating primary rat retinal cells and MT3-KO mouse

astrocytes with 5 μM pyrithione for the indicated times, with or without additional 500 nM Zn, after which they were stained with the Zn-specific fluorescent dye, FluoZin-3-AM (5 μM; Invitrogen), for 30 min at 37 °C and washed in serum-free MEM. Cells were observed under a fluorescence microscope and photographed ($n$ = 3).

### Statistical analysis

Differences in the incidence of grade 2B lesions and the appearance of a cavitation bubble between groups were analyzed by Fisher's exact test. All results are presented as mean ± SEM. Student's $t$-tests were used to evaluate the significance of differences between two groups. Values of $P < 0.05$ were considered significant. Graphical presentations were created using SigmaPlot version 10.0 software.

## Results

### Expression of MT3 in the retina

A qPCR analysis detected MT3 mRNA in WT mouse eyes (Fig. 1); as expected MT3-KO eyes showed no significant level of MT3 mRNA (not shown). Using the MT3 mRNA/β-actin mRNA ratio to compare the relative amount of mRNA among samples from various mouse organs, we found a modest level of MT3 mRNA (about 10% of that in the brain) in the whole eye of the WT mouse. Because eye samples contain vitreous and sclera, which are unlikely to contribute to MT3 expression, the level of MT3 mRNA determined in whole eyes underestimates that in the retina. In fact, when only retinal tissues were used, the level of MT3 mRNA was about 80% of that in the brain (81.2 ± 1.83%, $n$ = 3), indicating that most MT3 expression in the eye is likely in the retina.

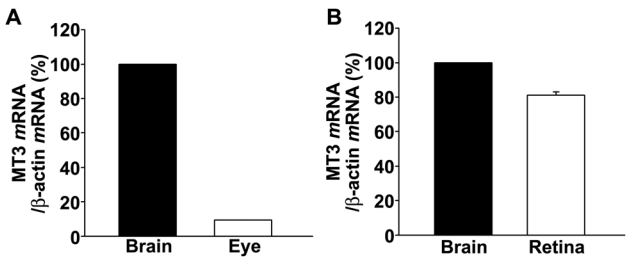


**Fig. 1** Estimated MT3 expression in the mouse retina. MT3 expression in mouse eyes and retinal cell cultures was quantified using RT-qPCR. (A) MT3 mRNA was detected at modest levels (about 10% of that in the brain) in the whole eye of the mouse. (B) MT3 mRNA was detected at relatively high levels (~80% of that in the brain) in retinal tissue, suggesting that most MT3 mRNA detected in whole eyes reflects retinal expression. Values are presented as means ± SD ($n$ = 3).

### Histological analysis of laser-induced CNV

Retinal sections were obtained 24 h after laser-treatment and stained with TFL-Zn. In MT3 WT mice, it was noted that intense zinc fluorescence appeared in cells and damaged tissue around the laser focus (Fig. 2A, arrows). In contrast, in MT3-KO mice, zinc fluorescence around the focus was less intense and less extensive.

To estimate the extent of CNV formation in these mice, retinal sections were obtained 2 weeks after the laser treatment (Fig. 2B). The morphological features of CNV lesions were similar in WT and MT3-KO mice. However, we found that CNV lesions in WT mice were significantly larger in width and height than those in MT3-KO mice (Fig. 2B, arrows). There was a discontinuity in Bruch's membrane in the area of each laser burn in all mice. Fibrovascular tissue, retinal pigment epithelial (RPE) cells, pigment clumping, and atrophy of overlying photoreceptor layers could be observed in the area of CNV in both WT and MT3-KO retinas.

### Leakage from CNV

The frequencies of laser-induced (200 mW) cavitation bubbles in WT (83.5%) and MT3-KO (91.5%) mice were not significantly different ($P > 0.05$). Hemorrhagic complications occurred only in six of all burns (two in the WT group and four in the KO group). A comparison of lesion size and the severity of leakage

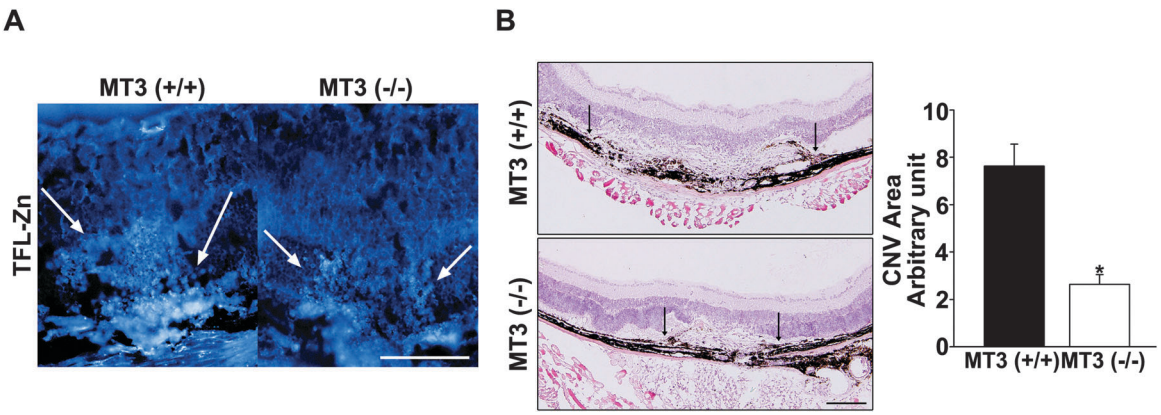


**Fig. 2** Histological evaluation of CNV size in WT and MT3-KO mice. (A) TFL-Zn (0.1 mM in PBS, pH 8.0) staining of retinas 24 h after laser treatment in WT mice and MT3-KO mice. Around the laser injury focus WT mice exhibited intense and extensive zinc fluorescence (arrows). In contrast, MT3-KO retinas showed less zinc fluorescence. Original magnification, ×200; scale bar, 100 μm. (B) H&E staining of retinas 2 weeks after laser injury confirmed that CNV lesions in MT3-KO mice were less severe than those in WT mice (WT = 4, KO = 5). Arrows indicate the extent of CNV. Morphologic features of the CNV lesions were similar in WT and MT3-KO mice and consisted of fibrovascular tissue, RPE cells, and pigment clumping. Atrophy of overlying photoreceptor layers could be observed. Original magnification, ×100; scale bar, 100 μm.

 

in fluorescein angiograms revealed that CNV lesions in MT3-KO mice were smaller and less leaky than those in WT mice (Fig. 3). At day 14, pathologically significant leakage (grade 2B lesions) was observed in 55.8% of lesions in WT mice, but developed at a significantly lower rate (10.6%) in MT3-KO mice ($P < 0.05$; Fig. 4A).

**Size and vascularity of CNV.** Next, we estimated the size and vascularity of CNV lesions using images obtained by FA using a Micron III system. CNV lesions were markedly larger in WT mice than in MT3-KO mice ($P < 0.01$; Fig. 4B). Similarly, the vascularity of CNV lesions was significantly greater in WT mice than in MT3-KO mice ($P < 0.005$; Fig. 4C).

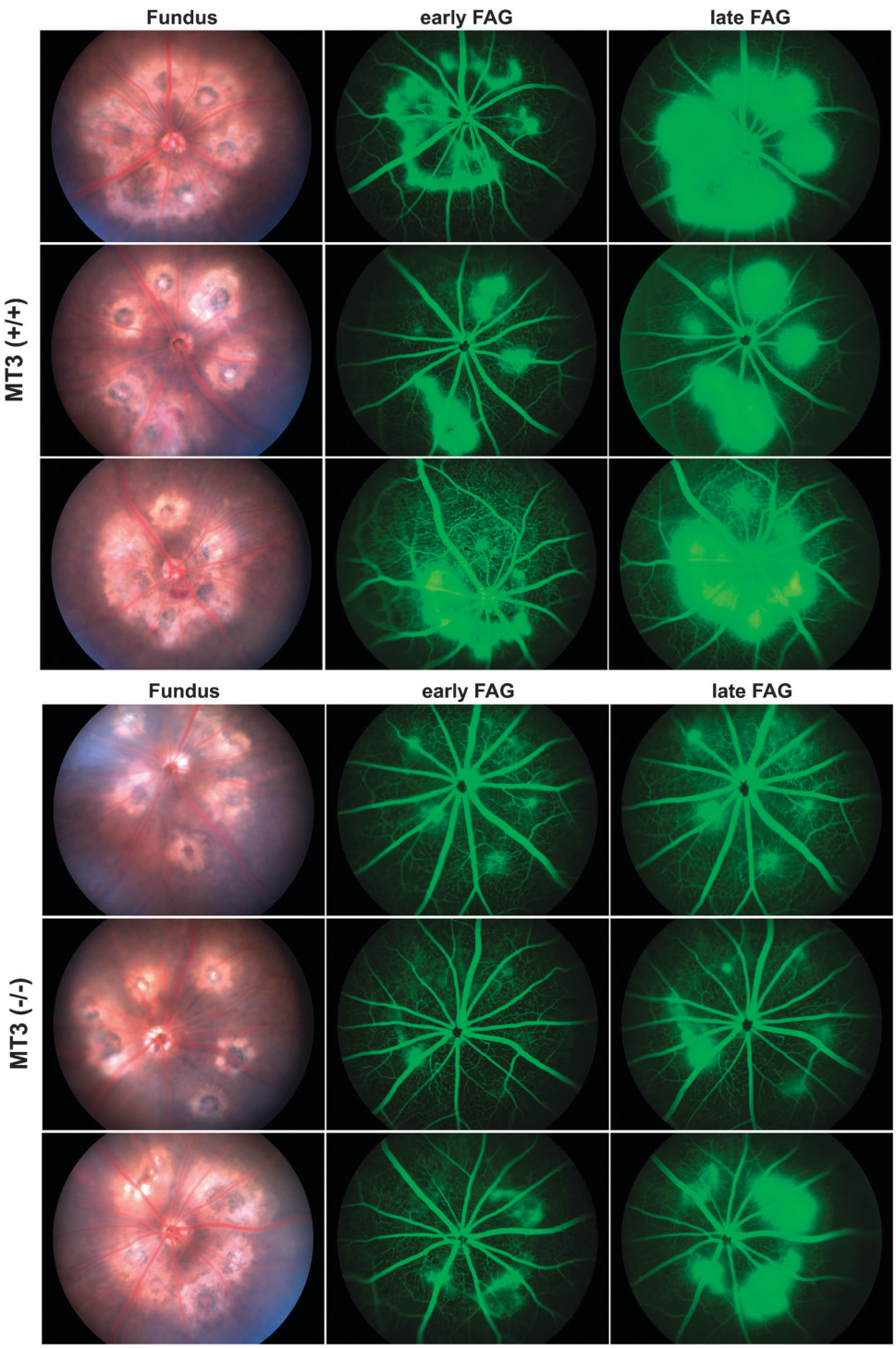


**Fig. 3** Representative early- and late-phase fundus fluorescein angiograms. Photographs taken 2 weeks after laser treatment (200 mW) showed that WT mice developed larger CNV lesions (fundus, early FA) and showed more progressive angiographic leakage (late FA) compared to MT3-KO mice.

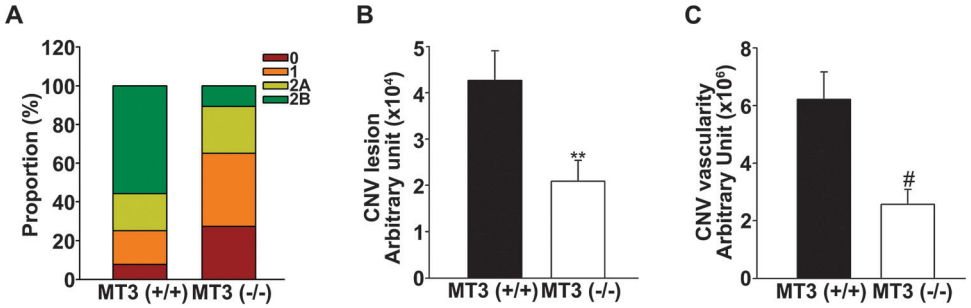


**Fig. 4** Grading angiographic leakage and quantification of CNV size and vascularity. (A) The percentage of each lesion grade in WT ($n$ = 5, spot = 52) and MT3-KO ($n$ = 6, spot = 66) retinas detected 2 weeks after laser induction is presented as histograms. The percentage of grade 2B lesions was greater in WT than in MT3-KO mice. 0 (not leaky), 1 (questionable leakage), 2A (leaky), 2B (pathologically significant leakage). CNV lesion size (B) and vascularity (C) were quantified in WT ($n$ = 5) and MT3-KO ($n$ = 6) mice using Micron III fluorescein angiograms. CNV lesions were larger and showed higher relative intensity of fluorescence in WT mice than in MT3-KO mice. Size and vascularity of CNV were determined by computer-assisted image analysis and differed significantly between groups (**$P < 0.01$ and $^{\#}P < 0.005$, two tailed $t$ test).

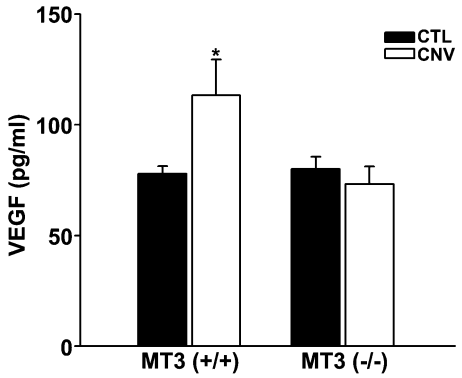


**Fig. 5** Quantification of VEGF protein levels by ELISA. VEGF protein levels in WT and MT3-KO mouse eyes were quantified by ELISA before and after laser induction of CNV. Bars denote VEGF levels (means ± SEM, pg ml$^{-1}$) in the retinas of WT ($n$ = 7) and MT3-KO ($n$ = 5) mice 2 weeks after laser treatment compared to those in controls ($n$ = 13, 12). The basal level of VEGF (*i.e.*, before laser injury) did not differ between WT and MT3-KO mice. Two weeks following induction of CNV using argon laser photocoagulation, VEGF levels in the eyes of WT group animals had increased from 77 pg ml$^{-1}$ to 113 pg ml$^{-1}$, whereas those in the eyes of MT3-KO group mice remained unchanged (*$P < 0.05$ compared to control).

### No VEGF induction following laser injury in MT3-KO eyes

We analyzed changes in VEGF levels following laser injury in both WT and MT3-KO eyes by ELISA (Fig. 5). The basal level of VEGF before laser injury did not differ between WT and MT3-KO groups. Two weeks following induction of CNV using argon laser photocoagulation, VEGF levels in the eyes of the WT group increased from 77 ± 3.39 pg ml$^{-1}$ to 113 ± 16.32 pg ml$^{-1}$, a difference that was statistically significant. In contrast, VEGF levels in the eyes of MT3-KO group animals remained unchanged.

Using Western blotting, we then analyzed the levels of hypoxia-inducible factor (HIF)-1α, a regulatory protein involved in the induction of VEGF, in laser-treated eyes and control eyes of WT and MT3-KO mice. In addition, we measured the levels of VEGF and the VEGF receptor, Flk-1. Flk-1 is the main receptor for VEGF, and pFlk-1 is the activated (phosphorylated) form. As shown in Fig. 6, HIF-1α and VEGF were readily detectable in both WT and KO tissues before laser treatment. Following laser treatment, the levels of HIF-1α and VEGF were significantly increased in WT tissues but not in MT3-KO tissues. Flk-1 levels increased in both WT and MT3-KO eyes following laser treatment, indicating that its induction is not likely dependent upon MT3.

### The role of Zn release in VEGF induction in retinal cells and MT3-KO astrocytes

In primary retinal cell cultures, adding 40 μM Zn to media increased intracellular Zn levels, visualized by monitoring FluoZin-3-AM, 30 min to 1 h after addition (Fig. 7A). Concomitantly, VEGF levels increased as assessed by immunoblotting (Fig. 7B). To examine whether the Zn effect was extracellular or intracellular, we used the known Zn ionophore, pyrithione.[28,29] Treatment for 30 min with 5 μM pyrithione, alone or with the addition of 500 nM Zn in the media, increased intracellular Zn levels in association with an increase in the levels of VEGF (Fig. 7C and D). Pyrithione is a zinc ionophore that greatly facilitates zinc entry; therefore, in order to observe a comparable effect of zinc in a cell culture, a significantly smaller amount of zinc should be used when pyrithione is present in the media. In our culture system, zinc at 500 nM with pyrithione had a similar effect as did zinc alone at 40 μM. The increase in VEGF induced by zinc or zinc plus pyrithione was completely blocked by the addition of 1 μM *N*,*N*,*N*′,*N*′-tetrakis(–)(2 pyridylmethyl)-ethylenediamine (TPEN), a cell-permeable Zn chelator. Finally, we examined whether an increase in intracellular Zn could induce VEGF in MT3-KO cells. Here, we used cortical astrocytes, as these cells were easier to obtain and maintain in culture than primary retinal cells. Western blot analyses showed that exposure to 40 μM Zn or pyrithione plus Zn increased intracellular Zn levels in MT3-KO astrocytes in association with an increase in the levels of VEGF and pFlk-1 (Fig. 8). Again, the addition of 1 μM TPEN blocked the increase in Zn and VEGF.

## Discussion

The present results demonstrate that MT3, a Zn-binding metallothionein that is primarily expressed in brain cells, is also expressed in the retina, and its absence markedly reduces the vulnerability of mouse eyes to laser-induced CNV formation.

 

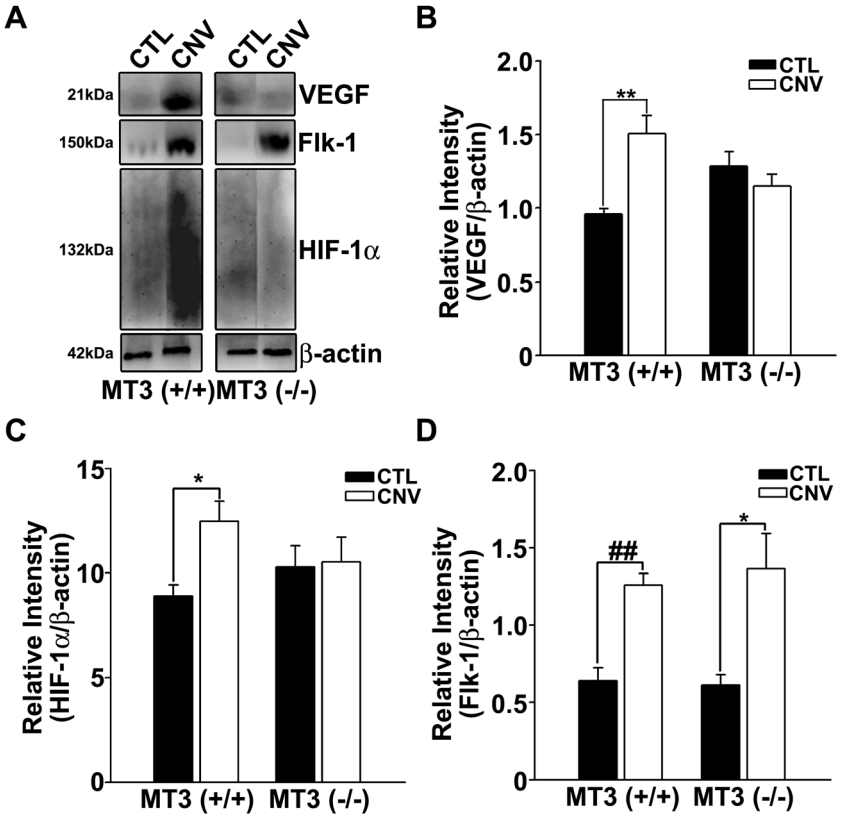


**Fig. 6** Analysis of HIF-1α, VEGF, and Flk-1 expression by Western blotting. Western blot analysis of HIF-1α, VEGF, and Flk-1 expression in WT (CTL = 4, CNV = 6) and MT3-KO (CTL = 3, CNV = 4) eye tissues before and 2 weeks after laser treatment. (A) Representative immunoblot. (B–D) Densitometric analysis. Compared with basal levels, HIF-1α and VEGF levels were significantly increased following laser treatment in WT retinas but not in MT3-KO retinas, whereas Flk-1 levels were increased to a similar extent in both WT and MT3-KO eyes following laser treatment (**$P < 0.01$, *$P < 0.05$, ##$P < 0.001$).

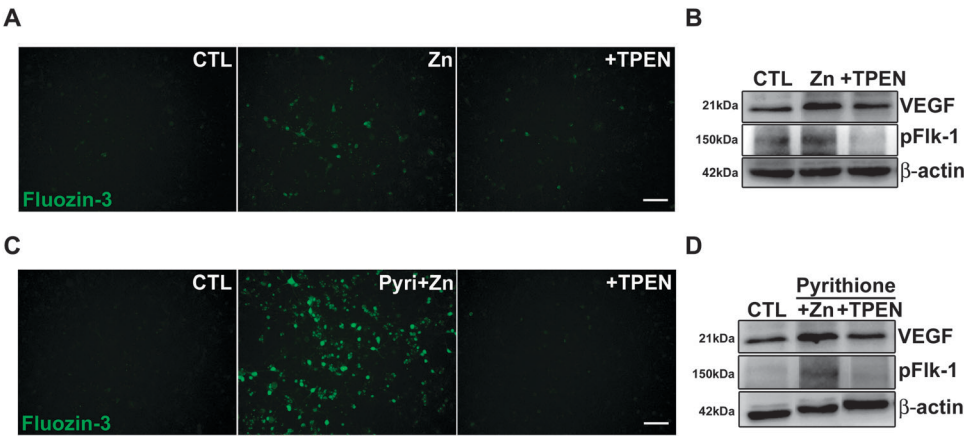


**Fig. 7** Induction of VEGF by increasing intracellular Zn levels. (A) FluoZin-3 fluorescence images obtained following Zn exposure. Addition of TPEN (stock: 100 μM in DMSO, final conc.: 1 μM) completely blocked the increase in Zn levels ($n = 3$). (B) Immunoblotting for VEGF after Zn treatment in retinal cultures. One hour after treatment with Zn (40 μM), the level of VEGF was increased. Pretreatment for 30 min with 1 μM TPEN completely blocked the increase ($n = 4$). (C) FluoZin-3 fluorescence images obtained following exposure to 5 μM pyrithione (Zn ionophore) or pyrithione plus zinc. Addition of TPEN completely blocked the increase in Zn levels ($n = 3$). (D) Immunoblot analysis and fluorescence photomicrographs of FluoZin-3-stained rat retinal cultures exposed to 5 μM pyrithione or pyrithione plus zinc. Intracellular Zn increase correlated with the increase in the levels of VEGF. Pretreatment for 30 min with 1 μM TPEN blocked the increase ($n = 3$).

Although establishing the detailed mechanisms will require further investigation, the present results suggest that the intracellular Zn release from MT3 triggered by laser injury contributes to the activation of the VEGF system in the retina. The level of HIF-1α, which promotes VEGF induction, as well as the level of VEGF increased in an MT3- and Zn-dependent manner.

The pathogenesis of CNV is not yet fully understood, although several potential mechanisms have been proposed.

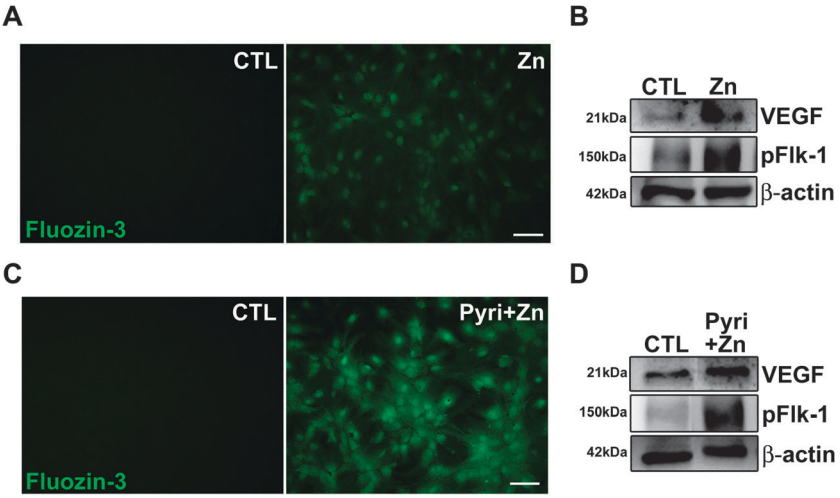


**Fig. 8** Immunoblot analysis and fluorescence photomicrographs of FluoZin-3-stained MT3-KO astrocytes. (A and C) Fluorescence photomicrographs of FluoZin-3-stained MT3-KO astrocyte cultures exposed to different Zn environments. Cells were sham washed (CTL) or treated for 1 h with 40 μM Zn (A), or for 1 h with 5 μM pyrithione plus 500 nM Zn (C). Western blots demonstrated that VEGF levels increased in MT3-KO astrocytes 1 h after treatment with Zn (40 μM) (B) or Zn plus pyrithione (5 μM) (D).

Normally, endothelial cells that line the ocular blood vessels are relatively impervious to neovascularization; thus, baseline endothelial cell proliferation is considered negligible. This quiescent state is attributed to a balance between the influences of proangiogenic (*e.g.*, VEGF) and antiangiogenic (*e.g.*, pigment epithelium-derived factor [PEDF]) factors. For angiogenesis to occur, the angiogenic molecular machinery must override the anti-angiogenic influences (*e.g.*, VEGF > PEDF).[30] Of the numerous angiogenesis-stimulating and -inhibiting factors, VEGF has been shown to be a crucial player in the formation of CNV; as such, anti-VEGF antibodies have been used to treat CNV lesions in patients with wet AMD.[31,32] Hence, understanding the pathogenic mechanisms underlying VEGF induction in CNV is necessary for the design of future therapeutic strategies.

In general, the function of MT3, which is preferentially expressed in the CNS, is largely unknown. However, MT3 mRNA levels change in response to CNS injury,[33–37] suggesting a role for MT3 in neuronal injury. A possible role in angiogenesis, which is thought to contribute to neuroprotection, was suggested by Kim *et al.*,[38] who reported that MT3 markedly induces HIF-1α and VEGF expression. Another report by Penkowa *et al.*[39] indicated that reduced levels of trophic factors, including VEGF, result in decreased angiogenesis and regeneration in the MT1/2-KO mice brain after a freeze lesion. Against this backdrop, we hypothesized that MT3 might play a role in retinal/choroidal angiogenesis.

Since there were no clear reports in the literature regarding the expression of MT3 in retina, we first performed a qPCR analysis and confirmed the presence of MT3 mRNA in the eyes of WT mice. Because the level of MT3 mRNA in the eye as a whole was low compared to that in the brain and because of difficulties in separating pure retinal tissue from the mouse eye, we utilized cultured rat retinal cells to establish MT3 levels in the retina. In rat retinal cultures, the level of MT3 mRNA was about 80% of that in the brain, indicating that most MT3 mRNA detected in the whole eye likely reflects expression in the retina. Unfortunately, our antibodies were not suitable for measuring MT3 protein levels.

Using a specific retinal imaging system for the mouse eye (Micron III) to acquire high-resolution fluorescein angiograms, we were able to observe time-dependent, dynamic changes in fundus fluorescence. CNV size could be assessed in early FA images obtained before substantial leakage of fluorescein. Because fluorescein diffused out of vessels in the late phase, demarcating the fluorescein leakage from CNV was not possible, and we used peak-phase FA images to assess CNV vascularity and leakage. These measurements revealed that CNV lesions in WT mice were larger and showed greater vascularity than those in MT3-KO mice, indicating less severe CNV formation in MT3-KO mice. The implication of these observations is that MT3 contributes to CNV.

As noted above, considerable evidence suggests that VEGF plays a critical role in CNV formation. Consistent with this, we found that the increase in VEGF in the retina of MT3-KO mice 2 weeks after laser treatment was substantially less than that in WT mice. Moreover, the level of HIF-1α, an upstream regulator of VEGF expression, was also increased only in WT retinas following injury, indicating that HIF-1α expression in injured retina is likely MT3 dependent. Interestingly, the levels of Flk-1, the main receptor for VEGF, were increased in both WT and MT3-KO eyes, indicating that Flk-1 induction was independent of MT3.

MT3 is known to regulate intracellular Zn levels by binding or releasing Zn, depending on the milieu. For instance, the oxidative stress that often accompanies injury releases Zn from MT3.[40–42] Consistently, we found in the present study that the zinc accumulation in retinal cells around the laser injury was significantly reduced in MT3-KO mice (Fig. 2A). Hence, it is

 

possible that an increase in the intracellular Zn level originating from MT3, rather than MT3 protein *per se*, may cause VEGF induction. Consistent with this possibility, raising intracellular Zn was sufficient to induce VEGF in retinal cell cultures. Furthermore, even in MT3-KO astrocytes, zinc or zinc plus pyrithione robustly induced VEGF and activated Flk-1. In both cases, the increase in VEGF levels was completely blocked by TPEN, an intracellular Zn chelator.

## Conclusions

Taken together, the results presented here demonstrate that MT3 plays a role in injury-induced CNV formation in the mouse retina, likely by releasing Zn and inducing VEGF. Thus, measures to reduce Zn release from MT3 may be helpful in reducing CNV formation in human eye diseases, such as AMD.

## Acknowledgements

This work was supported by National Research Foundation of Korea (NRF): 2005-0093836; Original Technology Research Program for Brain Science: 2009-0081487; Korean health Technology R&D project, Ministry of Health & Welfare (KHIDI): A092042; and Asan Institute for Life Sciences: 2012-193.

## References

1 N. M. Bressler, S. B. Bressler, N. G. Congdon, F. L. Ferris, 3rd, D. S. Friedman, R. Klein, A. S. Lindblad, R. C. Milton and J. M. Seddon, *Arch. Ophthalmol.*, 2003, **121**, 1621–1624.
2 D. S. Friedman, B. J. O'Colmain, B. Munoz, S. C. Tomany, C. McCarty, P. T. de Jong, B. Nemesure, P. Mitchell, J. Kempen and G. Eye Diseases Prevalence Research, *Arch. Ophthalmol.*, 2004, **122**, 564–572.
3 M. M. Brown, G. C. Brown, S. Sharma, J. D. Stein, Z. Roth, J. Campanella and G. R. Beauchamp, *Curr. Opin. Ophthalmol.*, 2006, **17**, 257–266.
4 N. S. Bora, S. Kaliappan, P. Jha, Q. Xu, J. H. Sohn, D. B. Dhaulakhandi, H. J. Kaplan and P. S. Bora, *J. Immunol.*, 2006, **177**, 1872–1878.
5 P. S. Bora, J. H. Sohn, J. M. Cruz, P. Jha, H. Nishihori, Y. Wang, S. Kaliappan, H. J. Kaplan and N. S. Bora, *J. Immunol.*, 2005, **174**, 491–497.
6 P. A. Campochiaro, *J. Cell. Physiol.*, 2000, **184**, 301–310.
7 F. L. Ferris, 3rd, S. L. Fine and L. Hyman, *Arch. Ophthalmol.*, 1984, **102**, 1640–1642.
8 D. Husain, B. Ambati, A. P. Adamis and J. W. Miller, *Ophthalmol. Clin. North Am.*, 2002, **15**, 87–91.
9 S. J. Ryan, *Arch. Ophthalmol.*, 1982, **100**, 1804–1809.
10 J. R. Yates and A. T. Moore, *J. Med. Genet.*, 2000, **37**, 83–87.
11 P. A. Campochiaro, *Expert Opin. Biol. Ther.*, 2004, **4**, 1395–1402.
12 S. J. Song, H. Chung and H. G. Yu, *Ophthalmic Res.*, 2008, **40**, 35–40.
13 A. Bikfalvi and R. Bicknell, *Trends Pharmacol. Sci.*, 2002, **23**, 576–582.
14 M. Cristofanilli, C. Charnsangavej and G. N. Hortobagyi, *Nat. Rev. Drug Discovery*, 2002, **1**, 415–426.
15 R. K. Jain, *Nat. Med.*, 2003, **9**, 685–693.
16 D. M. Brown, P. K. Kaiser, M. Michels, G. Soubrane, J. S. Heier, R. Y. Kim, J. P. Sy, S. Schneider and A. S. Group, *N. Engl. J. Med.*, 2006, **355**, 1432–1444.
17 P. J. Rosenfeld, D. M. Brown, J. S. Heier, D. S. Boyer, P. K. Kaiser, C. Y. Chung, R. Y. Kim and M. S. Group, *N. Engl. J. Med.*, 2006, **355**, 1419–1431.
18 S. Rofagha, R. B. Bhisitkul, D. S. Boyer, S. R. Sadda, K. Zhang and S.-U. S. Group, *Ophthalmology*, 2013, DOI: 10.1016/j.ophtha.2013.03.046.
19 J. H. Kagi and Y. Kojima, *Experientia, Suppl.*, 1987, **52**, 25–61.
20 R. D. Palmiter, S. D. Findley, T. E. Whitmore and D. M. Durnam, *Proc. Natl. Acad. Sci. U. S. A.*, 1992, **89**, 6333–6337.
21 B. A. Masters, C. J. Quaife, J. C. Erickson, E. J. Kelly, G. J. Froelick, B. P. Zambrowicz, R. L. Brinster and R. D. Palmiter, *J. Neurosci.*, 1994, **14**, 5844–5857.
22 I. Hozumi, J. S. Suzuki, H. Kanazawa, A. Hara, M. Saio, T. Inuzuka, S. Miyairi, A. Naganuma and C. Tohyama, *Neurosci. Lett.*, 2008, **438**, 54–58.
23 K. S. Gurusamy, N. Farooqui, M. Loizidou, S. Dijk, J. W. Taanman, S. Whiting, M. J. Farquharson, B. J. Fuller and B. R. Davidson, *Biometals*, 2011, **24**, 143–151.
24 J. C. Erickson, G. Hollopeter, S. A. Thomas, G. J. Froelick and R. D. Palmiter, *J. Neurosci.*, 1997, **17**, 1271–1281.
25 E. Sakurai, H. Taguchi, A. Anand, B. K. Ambati, E. S. Gragoudas, J. W. Miller, A. P. Adamis and J. Ambati, *Invest. Ophthalmol. Visual Sci.*, 2003, **44**, 2743–2749.
26 T. Y. Kim, J. S. Yi, S. J. Chung, D. K. Kim, H. R. Byun, J. Y. Lee and J. Y. Koh, *Exp. Neurol.*, 2007, **208**, 159–167.
27 Y. H. Yoon, K. H. Jeong, M. J. Shim and J. Y. Koh, *Brain Res.*, 1999, **823**, 33–41.
28 M. H. Park, S. J. Lee, H. R. Byun, Y. Kim, Y. J. Oh, J. Y. Koh and J. J. Hwang, *Neurobiol. Dis.*, 2011, **42**, 242–251.
29 I. J. Forbes, P. D. Zalewski and C. Giannakis, *Exp. Cell Res.*, 1991, **195**, 224–229.
30 J. Z. Nowak, *Pharmacol. Rep.*, 2006, **58**, 353–363.
31 N. Shams and T. Ianchulev, *Ophthalmol. Clin. North Am.*, 2006, **19**, 335–344.
32 A. Kvanta, P. V. Algvere, L. Berglin and S. Seregard, *Invest. Ophthalmol. Visual Sci.*, 1996, **37**, 1929–1934.
33 T. Anezaki, H. Ishiguro, I. Hozumi, T. Inuzuka, M. Hiraiwa, H. Kobayashi, T. Yuguchi, A. Wanaka, Y. Uda and T. Miyatake, *et al.*, *Neurochem. Int.*, 1995, **27**, 89–94.
34 I. Hozumi, T. Inuzuka, M. Hiraiwa, Y. Uchida, T. Anezaki, H. Ishiguro, H. Kobayashi, Y. Uda, T. Miyatake and S. Tsuji, *Brain Res.*, 1995, **688**, 143–148.
35 T. Yuguchi, E. Kohmura, K. Yamada, T. Sakaki, T. Yamashita, H. Otsuki, K. Kataoka, S. Tsuji and T. Hayakawa, *J. Neurotrauma*, 1995, **12**, 299–306.
36 T. Inuzuka, I. Hozumi, A. Tamura, M. Hiraiwa and S. Tsuji, *Brain Res.*, 1996, **709**, 151–153.

37 L. Acarin, J. Carrasco, B. Gonzalez, J. Hidalgo and B. Castellano, *J. Neuropathol. Exp. Neurol.*, 1999, **58**, 389–397.
38 H. G. Kim, Y. P. Hwang and H. G. Jeong, *Biochem. Biophys. Res. Commun.*, 2008, **369**, 666–671.
39 M. Penkowa, J. Carrasco, M. Giralt, A. Molinero, J. Hernandez, I. L. Campbell and J. Hidalgo, *J. Cereb. Blood Flow Metab.*, 2000, **20**, 1174–1189.
40 M. Aschner, M. G. Cherian, C. D. Klaassen, R. D. Palmiter, J. C. Erickson and A. I. Bush, *Toxicol. Appl. Pharmacol.*, 1997, **142**, 229–242.
41 R. D. Palmiter, *Proc. Natl. Acad. Sci. U. S. A.*, 1998, **95**, 8428–8430.
42 S. J. Lee, M. H. Park, H. J. Kim and J. Y. Koh, *Glia*, 2010, **58**, 1186–1196.



 